JACS
JOURNAL OF THE AMERICAN CHEMICAL SOCIETY

Article

pubs.acs.org/JACS

Small-Molecule Binding Sites on Proteins Established by Paramagnetic NMR Spectroscopy

Jia-Ying Guan,[†] Peter H. J. Keizers,[†] Wei-Min Liu,[†] Frank Löhr,[‡] Simon P. Skinner,[†] Edwin A. Heeneman,[†] Harald Schwalbe,[§] Marcellus Ubbink,*[,†] and Gregg Siegal*[,†]

[†]Gorlaeus Laboratories, Leiden Institute of Chemistry, Leiden University, Post Office Box 9502, 2300 RA Leiden, The Netherlands
[‡]Institute of Biophysical Chemistry and [§]Institute of Organic Chemistry and Chemical Biology, Goethe University Frankfurt and Center for Biomolecular Magnetic Resonance, Max-von-Laue Strasse 7, 60438 Frankfurt am Main, Germany

Supporting Information

ABSTRACT: Determining the three-dimensional structure of a small molecule−protein complex with weak affinity can be a significant challenge. We present a paramagnetic NMR method to determine intermolecular structure restraints based on pseudocontact shifts (PCSs). Since the ligand must be in fast exchange between free and bound states and the fraction bound can be as low as a few percent, the method is ideal for ligands with high micromolar to millimolar dissociation constants. Paramagnetic tags are attached, one at a time, in a well-defined way via two arms at several sites on the protein surface. The ligand PCSs were measured from simple 1D ^{1}H spectra and used as docking restraints. An independent confirmation of the complex structure was carried out using intermolecular NOEs. The results show that structures derived from these two approaches are similar. The best results are obtained if the magnetic susceptibility tensors of the tags are known, but it is demonstrated that with two-armed probes, the magnetic susceptibility tensor can be predicted with sufficient accuracy to provide a low-resolution model of the ligand orientation and the location of the binding site in the absence of isotope-labeled protein. This approach can facilitate fragment-based drug discovery in obtaining structural information on the initial fragment hits.

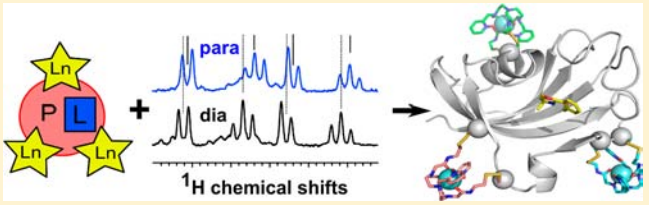

INTRODUCTION

The availability of three-dimensional structures of protein−ligand complexes significantly improves the efficiency of refining hits toward leads in the early stages of drug discovery.[1] Typically, structure-driven hit optimization programs rely on crystallographic data. In fragment-based drug discovery (FBDD), however, weakly binding ligands (fragments) are often not observed in crystals, for a variety of reasons. NMR spectroscopy is a powerful alternative for deriving structural information, particular for weakly interacting complexes. The classical NMR approach is based on the observation of intermolecular NOEs and is suitable for most proteins smaller than 40 kDa. Although robust, the method can be time-consuming and requires uniformly isotopically labeled protein. The method is strictly limited to proteins that can be functionally expressed under these conditions. Selective isotope labeling schemes have been employed in combination with deuteration to enable NMR analysis of much larger proteins. Complexation-induced chemical shift perturbation (CSP) data have been used as ambiguous interaction constraints to calculate structures of protein−ligand complexes.[2] However, this method monitors both direct and remote effects, and therefore the binding site is not always well defined. We sought a method that could in principle be applied to proteins where no, or only limited, isotope labeling can be performed.

Paramagnetic NMR is known to be a powerful tool to study biological systems due to its versatile effects, including pseudocontact shifts (PCSs), paramagnetic relaxation enhancement (PRE), and residual dipolar coupling (RDC).[3−5] Paramagnetic NMR has been applied extensively to characterize protein−protein interactions, but very little in protein−small molecule interactions. Pioneer studies used the PRE caused by a paramagnetic metal ion[6] or spin label[7,8] to facilitate ligand screening and potentially, to obtain information on the ligand pose.[6] A combination of PCS and RDC was applied to assist structure determination of a carbohydrate−protein complex where the paramagnetic center was introduced by creating a fusion protein with a C-terminal lanthanide-binding peptide tag (LBT).[9] PRE-assisted ligand docking with a spin-labeled peptide bound specifically to a protein was also reported.[10] Recently, paramagnetic effects stemming from a two-point anchored N-terminal LBT were used to determine the structure of protein−peptide complexes.[11] PCSs have also been applied to determine the structure of a small-molecule ligand in rapid exchange with a protein in which a lanthanide was bound in a natural metal binding site.[12] In this study the ligand bound very closely to the lanthanide, enabling the use of large ligand-to-protein ratios. This latter example is the only case where PCSs

Received: February 5, 2013
Published: March 20, 2013

   dx.doi.org/10.1021/ja401323m | J. Am. Chem. Soc. 2013, 135, 5859−5868

have been used to elucidate the structure of a protein−ligand complex containing a small fragment (M_w < 300 Da).

We demonstrate here an alternative way to determine the location and orientation of a weakly bound fragment with PCS restraints from a ligand in rapid exchange with a protein. A rigid, double-armed lanthanide-binding tag, CLaNP-5,[13,14] was attached at three different sites, one at a time, on the protein surface via disulfide bond linkage. Using this tag, the magnitude and orientation of the $\Delta\chi$-tensors can be predicted. Further, the paramagnetic effects can be tuned by using different lanthanides in the tag. We selected FKBP12 as a model protein to investigate the potential of the methodology. FKBP12 is a peptidyl-prolyl isomerase which belongs to the family of immunophilins and is a drug target for the immunosuppressants rapamycin and FK506. There have been many structural studies on this protein.[15−20] The ligand in this study is a fragment that was identified as a hit against FKBP12 from a screen of a fragment library using target-immobilized NMR screening (TINS).[21] In this work, we compare the PCS-based docking result with the structure determined by intermolecular NOEs. The structure calculations were performed using parameters from both predicted and experimentally determined paramagnetic $\Delta\chi$-tensors. The result shows that, even without resonance assignments of the protein, it is possible to determine the ligand binding site and approximate orientation. The method can assist lead optimization in FBDD when high-resolution structural information is not available.

MATERIALS AND METHODS

Ligand Preparation. The ligand **1**, [2-(4,4-dimethyl-5,5-dihydro-1,3-oxazol-2-yl)phenyl]methanol, was purchased from MayBridge (catalog number S13756). Assignment of the ligand resonances was achieved from 2D ^{1}H, ^{13}C-HSQC and ^{1}H,^{13}C-HMBC spectra acquired on a 100 mM solution of the ligand in D_2O.

Protein Expression and Purification. Recombinant human FKBP12 wild-type and double cysteine mutants (K34C/K35C, K44C/K47C, C22V/E61C/Q65C), all of which contain an additional LEHHHHHH tag at the C-terminus, were purified from *Escherichia coli* strain BL21(DE3) containing the overexpression plasmid pET20b with FKBP12 insert. Uniformly ^{15}N-labeled and ^{15}N,^{13}C-labeled FKBP12 were purified from *E. coli* cells cultured in minimal media containing $^{15}NH_4Cl$ and $^{12}C_6$- or $^{13}C_6$-glucose, respectively. The bacterial culture was incubated at 37 °C until OD 0.6−0.8, and then gene expression was induced by adding IPTG to a final concentration of 1 mM. Incubation was continued at 18 °C overnight. After centrifugation, the pellets were resuspended in 5 mL/g pellet sucrose buffer (50 mM Tris, 20% sucrose, 1 mM EDTA, pH 7.5), centrifuged at 7000*g* for 30 min at 4 °C, resuspended in 5 mL/g pellet of 5 mM $MgSO_4$ and incubated on ice for 10 min. Cells were then centrifuged at 4500*g* for 20 min, the supernatant was discarded, and the pellet was resuspended in 1.5 mL/g pellet lysis buffer (50 mM sodium phosphate, 5 mM imidazole, 500 mM NaCl, pH 7.5) and frozen. For lysis, cell suspensions were incubated with PMSF, DNase, and lysozyme at room temperature for 1 h, and lysis was achieved using a French press (SLM Instruments Inc.). The crude lysate was cleared by ultracentrifugation at 35000*g* for 45 min at 4 °C, followed by filtration through a 0.22 μm syringe filter. FKBP12 was purified to homogeneity using a 5 mL His-Trap column (GE Healthcare) with a gradient of 5−500 mM imidazole, followed by a Superdex G75 gel filtration column (GE Healthcare). Protein concentrations were determined by UV−vis spectroscopy (ε_{280} = 9970 M^{-1} cm^{-1}). The purity was confirmed by SDS-PAGE and Comassie blue staining. The yield was in general 80 mg L^{-1} for wild-type FKBP12 and 15−23 mg L^{-1} for the double cysteine mutants.

CLaNP-5 Attachment. To a solution of FKBP12 double cysteine mutant in 25 mM sodium phosphate and 100 mM NaCl, pH 7.5, was added 10 mM dithiothreitol, and the reaction mixture was incubated on ice for 1 h to reduce cystines. After removal of DTT with a PD-10 column (GE Healthcare), 3−10 mol equiv of Ln^{3+}-CLaNP-5 were added to a 20 μM solution of the reduced FKBP12 and incubated on ice for 1 h. The mixture was purified using a PD-10 column followed by a 24 mL Superdex 75 gel filtration column (GE Healthcare) to separate the probe attached monomeric protein from dimers and excess probe. Protein concentrations were determined by UV−vis spectroscopy (ε_{280} = 9970 M^{-1} cm^{-1} for FKBP12 and 2200 M^{-1} cm^{-1} for CLaNP-5). The fractions of dimers were estimated to be 10%-25% based on the intensities observed on SDS-PAGE analysis. The yields of pure tagged proteins after purification were 20−40%.

NMR Measurements. All protein NMR samples contained 15 mM Tris-HCl, 25 mM NaCl, pH 7.7, and 6% D_2O for ^{15}N-labeled protein or >95% D_2O for non-isotope-labeled protein. The concentration of wild-type FKBP12 and Ln^{3+}-CLaNP-5-attached FKBP12 was 17−100 μM for titrations and 1.5 mM for resonance assignment and NOESY experiments. The ligand-to-protein ratio was 1.3:1 for all Ln^{3+}-CLaNP-5-attached FKBP12 mutants. 1D ^{1}H, [^{1}H,^{15}N]-HSQC, HNCA, HNCACB, HN(CO)CA, HN(CO)CACB, HNCO, (H)CCH-TOCSY, HN(CA)CO, and HBHA(CBCACO)NH spectra were recorded at 290 K on a Bruker Avance DMX-600 spectrometer equipped with a TCI-Z-GRAD cryoprobe. 1D ^{1}H NMR spectra of the complex CLaNP5-FKBP12 and ligand **1** were recorded at 600 MHz with a spectral width of 16 ppm and 6k complex points, resulting in a digital resolution of 1.56 Hz before zero filling. Carr−Purcell−Meiboom−Gill (CPMG) pulse sequence was used with a total echo time of 60 ms, comprising 60 pulses, for suppression of macromolecules resonances. A ligand-to-protein ratio of 10:1 was used in the 3D ^{15}N-separated ω1-^{13}C/^{15}N-filtered NOESY-TROSY, 3D NOESY-[^{1}H,^{15}N]-TROSY, 3D ^{13}C-separated ω1-^{13}C/^{15}N-filtered NOESY-[^{1}H,^{13}C]-HSQC, 3D NOESY-[^{1}H,^{13}C]-HSQC, and 2D ^{13}C-edited, ^{13}C/^{15}N-filtered NOESY, and a ratio of 3:1 was used in the 2D NOESY, 2D DQF-COSY, and 2D TOCSY spectra, recorded on a Bruker Avance 950 MHz spectrometer with a ^{1}H{^{13}C,^{15}N} cryogenic probe. Data were processed in TopSpin (Bruker), and then spectra were analyzed in Sparky.[22]

Calculations of Dissociation Constants and Bound Ligand Fractions. Ligand binding was observed via the changes of protein resonances in the [^{1}H,^{15}N]-HSQC spectrum upon titration with the ligand.[23] For analysis of the CSPs of ^{1}H and ^{15}N backbone resonances, the weighted average chemical shift values were calculated and normalized according to eq 1:

$$\Delta\delta_{avg} = \sqrt{\frac{1}{2}\left[\left(\frac{\Delta\delta_N}{5}\right)^2 + \Delta\delta_H{}^2\right]} \quad (1)$$

where $\Delta\delta_N$ and $\Delta\delta_H$ are the differences of ^{15}N and ^{1}H chemical shift of an amide group, respectively.

The dissociation constant (K_D) was determined using a two-parameter nonlinear regression curve fitting based on a one-site binding model as described in eq 2:

$$\Delta\delta_{avg} = \frac{1}{2}\Delta\delta_0(A^2 - 4R)$$
$$A = 1 + \frac{1}{R} + \frac{P_0R + L_0}{P_0L_0\left(\frac{1}{K_D}\right)} \quad (2)$$

where R is the total [ligand] to [protein] ratio, $\Delta\delta_{avg}$ is the average CSP (eq 1) at a given R, $\Delta\delta_0$ is the CSP at 100% bound protein, P_0 is the starting concentration of the protein, L_0 is the stock concentration of ligand, and K_D is the dissociation constant.[24] The fraction of bound ligand was calculated using the dissociation constant.

NOE-Based Structure Calculations. Intermolecular NOE cross-peaks were identified in 2D and 3D NOESY spectra with NOE mixing times of 50−70 ms and then converted into distances using the CYANA[25] calibration function. Intermolecular restraints were introduced as ambiguous restraints if degenerate protons were

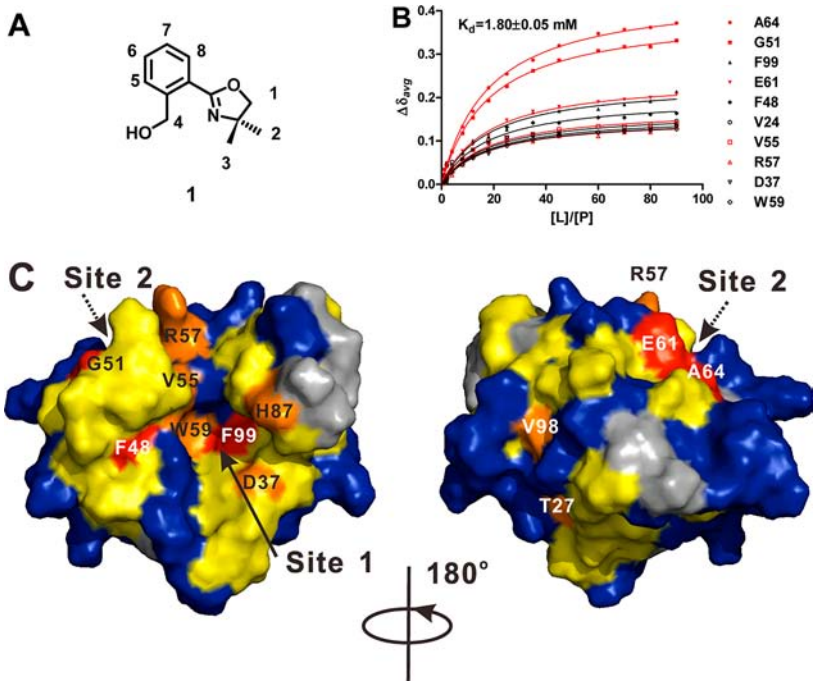

Figure 1. (A) Chemical structure of ligand **1**. (B) Chemical shift changes of FKBP12 resonances as a function of increasing [L]/[P]. The top 10 residues which showed largest perturbations are shown. Residues in the site-1 and site-2 regions are shown in black and red, respectively. The dissociation constant of **1** was obtained by fitting simultaneously to a 1:1 binding model (eq 2, solid lines). (C) Mapping of CSPs from the binding of **1** on the structure of FKBP12 (PDB entry 2PPN[27]). The positions of site 1 and site 2 are indicated. Color representation: red, $\Delta\delta_{avg} > 0.15$ ppm; orange, $0.15 > \Delta\delta_{avg} > 0.10$ ppm; yellow, $0.10 > \Delta\delta_{avg} > 0.03$ ppm; blue, $\Delta\delta_{avg} \leq 0.03$ ppm; dark gray, no data. Figures showing protein structures were prepared with PyMOL.[37]

involved or the protein resonance could not be unambiguously assigned.

Protein coordinates were taken from the X-ray and NMR structures of FKBP12 (PDB entries 1FKR,[15] 1FKS,[15] 1FKT,[15] 1D6O,[26] and 2PPN[27]), and the backbone was kept fixed throughout the process. Starting structures for the complex were generated by placing the ligand in random orientations with respect to FKBP12. Then the NOE distance restraints were applied to generate ligand orientations which satisfied the intermolecular restraints. Side-chain atoms within 8 Å of the ligand were allowed to rotate during subsequent energy minimization.

Magnetic Susceptibility Tensor Optimization and PCS-Based Structure Calculations. PCSs are defined as the difference in ppm between the corresponding resonance in the paramagnetic sample and the diamagnetic sample. The PCS gives information on the distance and angle between a nucleus and the paramagnetic center according to eq 3:[28]

$$\Delta\delta^{PCS} = \frac{1}{12\pi r^3}\left[\Delta\chi_{ax}(3\cos^2\theta - 1) + \frac{3}{2}\Delta\chi_{rh}\sin^2\theta\cos 2\varphi\right] \quad (3)$$

where r, θ, and φ are the polar coordinates of the nucleus with respect to the principle axes of the magnetic susceptibility anisotropy tensor ($\Delta\chi$-tensor), and $\Delta\chi_{ax}$ and $\Delta\chi_{rh}$ are the axial and rhombic components of the $\Delta\chi$-tensor, respectively. Errors were calculated by randomly excluding 10% of the data with Monte Carlo analysis implemented in Numbat.[29]

The fits of observed versus back-calculated protein PCSs and docking were performed in the XPLOR-NIH[30] program containing the PARArestraints module.[31] The predictions of the initial $\Delta\chi$-tensor positions and orientations were carried out as previously described.[14] The structure model, parameter, and topology files of the ligand were generated from the PRODRG server.[32] Bound ligand PCS values were used as the experimental restraints for PCS docking. PCSs of ligand methyl protons were used for methyl carbon positions instead of methyl proton positions. The protein backbone atoms and the pseudo-residues defining the metal coordinates were fixed in the docking process. The three data sets of the different tag positions on FKBP12 were used simultaneously. Ligand PCSs from all three tagging sites were used in the docking procedure with equal weighting. Each docking calculation comprised 100 steps, started with restrained rigid body docking for 20 steps (0.01 ps increments, 300 increment evaluations/step). The lowest energy structure was subsequently subjected to restrained Langevin dynamics for 80 steps (0.001 ps increments, 2000 increment evaluations/step), which allowed the ligand and the residues within 8 Å from the ligand to be flexible. A total of 200 independent docking calculations were performed using the solution structure of FKBP12 (PDB entry 1FKR, model 14)[15] and the predicted $\Delta\chi$-tensor parameters and position of the lanthanide ion. The same calculations with experimentally determined $\Delta\chi$-tensor parameters and positions were performed for comparison. The agreement between the experimental PCSs and back-calculated PCSs was evaluated using the Q factor defined in eq 4:[33]

$$Q = \sqrt{\frac{\sum_i (PCS_i^{exp} - PCS_i^{calc})^2}{\sum_i (|PCS_i^{exp}| + |PCS_i^{calc}|)^2}} \quad (4)$$

where PCS_i^{exp} and PCS_i^{calc} are the observed and calculated PCSs.

PCSdock Prediction. The PDB structure containing all three $\Delta\chi$-tensors (calculated or predicted) was imported into PCSdock (complete script provided in Supporting Information) using Scientific Python.[34] Ligand PCS data were imported, along with the axial and rhombic magnitudes of the $\Delta\chi$-tensors. A cubic grid of user-defined size (30 Å) was used, with 1 Å spacing placed around the protein using the center of mass as its origin. Predicted PCS values for the points on the grid were calculated for each paramagnetic $\Delta\chi$-tensor. The experimental ligand PCS values for an atom j were then compared to the predicted PCS values for each grid point i using a Q score defined by eq 5:

dx.doi.org/10.1021/ja401323m | J. Am. Chem. Soc. 2013, 135, 5859−5868

$$Q_{i,j} = \frac{1}{N}\sum_{k=1}^{N}\sqrt{\frac{(\mathrm{PCS}_{i,k}^{\mathrm{pred}} - \mathrm{PCS}_{j,k}^{\mathrm{exp}})^2}{(|\mathrm{PCS}_{i,k}^{\mathrm{pred}}| + |\mathrm{PCS}_{j,k}^{\mathrm{exp}}|)^2}} \quad (5)$$

where N is the number of paramagnetic $\Delta\chi$-tensors, $\mathrm{PCS}_{i,k}^{\mathrm{pred}}$ is the PCS calculated for the grid point i relative to the paramagnetic $\Delta\chi$-tensors k, and $\mathrm{PCS}_{j,k}^{\mathrm{exp}}$ is the experimental PCS used for the atom j relative to the paramagnetic $\Delta\chi$-tensors k. If the $Q_{i,j}$ for any atom of the ligand was lower than a user-defined level, the grid point i was accepted. If the $Q_{i,j}$ was larger for all atoms of the ligand, that grid point was discarded.

RESULTS

Characterization of the Ligand−Protein Interaction. The ligand **1** (Figure 1A) was identified from a TINS screen[21] of a library of commercially available, low-molecular-weight "drug fragments" for binding to FKBP12. To confirm the binding of **1** to FKBP12 and obtain structural insight into the binding site, we titrated the ligand into ^{15}N labeled protein and observed CSPs in a series of [^{1}H,^{15}N]-HSQC spectra with increasing ligand concentration. Figure 1B shows the titration curves for the ten residues most effected from which the equilibrium dissociation constant, K_D, could be extracted. CSPs occurred throughout the protein, including in two previously defined ligand binding sites, referred to as site-1 and site-2.[35] Five of these residues are site-1 residues and the other five residues belong to site-2. In Figure 1C the CSPs have been mapped onto the crystal structure of FKBP12 (PDB entry 2PPN[27]) and color-coded according to their magnitude. While CSPs can be caused by direct changes in the electronic environment of spins close to the ligand, many other factors can contribute. For example, it has been shown that, upon ligand binding to FKBP12, perturbations of both main-chain and side-chain dynamics can occur at sites distal to the binding interface.[36] Since such changes in dynamic behavior may also lead to CSPs, it was not possible to define the ligand binding site by CSP mapping alone. Therefore, we sought an alternative method to elucidate the structure of the complex.

NOE-Based Structure Calculations. The structure of the FKBP12−**1** complex was initially determined using standard intermolecular NOE based methods. *De novo* assignments of the complete protein were obtained. Backbone assignments (HN, CO, C_α, and C_β) of ligand-free protein were obtained from standard triple-resonance spectra and transferred to the bound state by following changes in [^{1}H,^{15}N]-HSQC and [^{1}H,^{13}C]-HSQC spectra upon ligand addition. Subsequently, the aliphatic side chains were assigned from a (H)CCH-TOCSY spectrum and the aromatic ones from 2D ^{1}H,^{1}H-NOESY, DQF-COSY, and ^{1}H,^{1}H-TOCSY spectra. Intermolecular NOEs were derived from a combination of 3D ^{15}N-separated ω1-^{13}C/^{15}N-filtered NOESY-TROSY, 3D NOESY-[^{1}H,^{15}N]-TROSY, 3D ^{13}C-separated ω1-^{13}C/^{15}N-filtered NOESY-[^{1}H,^{13}C]-HSQC, 3D NOESY-[^{1}H,^{13}C]-HSQC, 2D ^{13}C-edited, ^{13}C/^{15}N-filtered NOESY, and 2D NOESY spectra. Figures in the Supporting Information show regions of NOESY spectra containing intermolecular NOEs between the ligand and backbone amides (Figure S1) and side chains (Figure S2) of the protein. In total, 66 intermolecular NOE crosspeaks were identified in these NMR spectra, of which 43 restraints were used for structural calculations (Table S1). The NOEs that were weak (20 peaks) or with uncertain assignments (3 peaks) were excluded. Superposition of various FKBP12 structures from the PDB (1FKR, 1FKS, 1FKT, 1D6O, 2PPN) indicated that the loops surrounding the hydrophobic pocket are variable and hence might undergo significant dynamic behavior in solution. Therefore, to cover the range of conformations of the loops, multiple structures were used as input for structure calculations.

The position and orientation of the ligand is similar (Figures 2 and S3) in all structures, suggesting that the conformation of the loops does not strongly influence the protein−ligand interaction. A total of 33 out of 43 input NOEs were satisfied, resulting in a well-defined ligand orientation. However, some large violations of NOEs remain (Table S1 and Figure S4). The NOEs indicate 1 has contacts with residues located in site 1. The ligand interacts with the hydrophobic pocket formed by F36, F46, V55, I56, W59, I90, I91, and F99. The violations could be due to the motion of the flexible loop at residues 50−56 and 78−95, which are on opposite sides of the hydrophobic pocket.[18,36,38−40] As no single ligand orientation can satisfy all the restraints, it is possible that the dynamic behavior of the protein gives rise to time-averaged NOEs. Consistent with this idea, the backbone[18] and side chains[40] of FKBP12 were also shown previously to undergo chemical exchange on the μs-ms time scale. Alternatively, it is also possible that multiple ligand orientations are present. Therefore, the NOE structure presented here is only an approximation of the actual ligand binding mode. Analysis of the structures indicates possible hydrogen bonds present between (1) the ligand hydroxyl and Y82-hydroxyl, (2) the ligand hydroxyl and D37-Oδ, and (3) the ligand nitrogen and Y82-hydroxyl. Previous studies have suggested that the side chains of D37[19,41] and Y82[16] are involved in hydrogen-bonding with rapamycin and FK-506, two high-affinity ligands of FKBP12. Our NOE-based structure model shares a similar hydrogen-bonding framework with the previous studies.

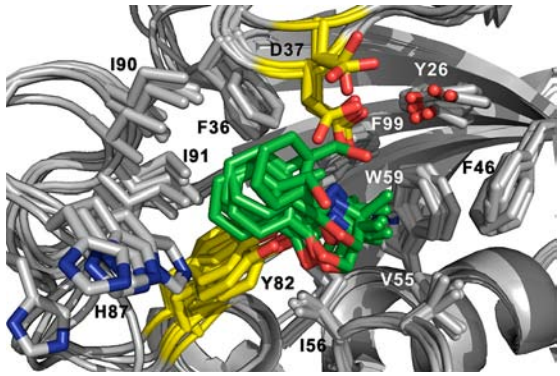

Figure 2. Overlay of the lowest energy structures of the complex of **1** (in green sticks) with 6 previously determined structures of FKBP12 (1D6O, 1FKR models 14 and 16, 1FKS, 1FKT, and 2PPN) as determined by intermolecular NOE restraints. The RMSD of all ligand atoms relative to the mean is 1.1 ± 0.4 Å. The side chains showing possible hydrogen bonding to ligand **1** are colored in yellow. The side chains of other residues showing intermolecular NOEs to the ligand are colored gray. Each individual structure is presented in Figure S3 in the Supporting Information.

Ligand Conformation. There are two possible orientations of the five-membered oxazole ring relative to the six-membered aromatic ring. Between these two orientations, the five-membered ring flips by 180°. The difference in intensities of intramolecular NOEs between protons 4/1, 4/2, and 4/3 (proton numbers as indicated on the structure in Figure 1A) in the presence of FKBP12 suggests that the presented

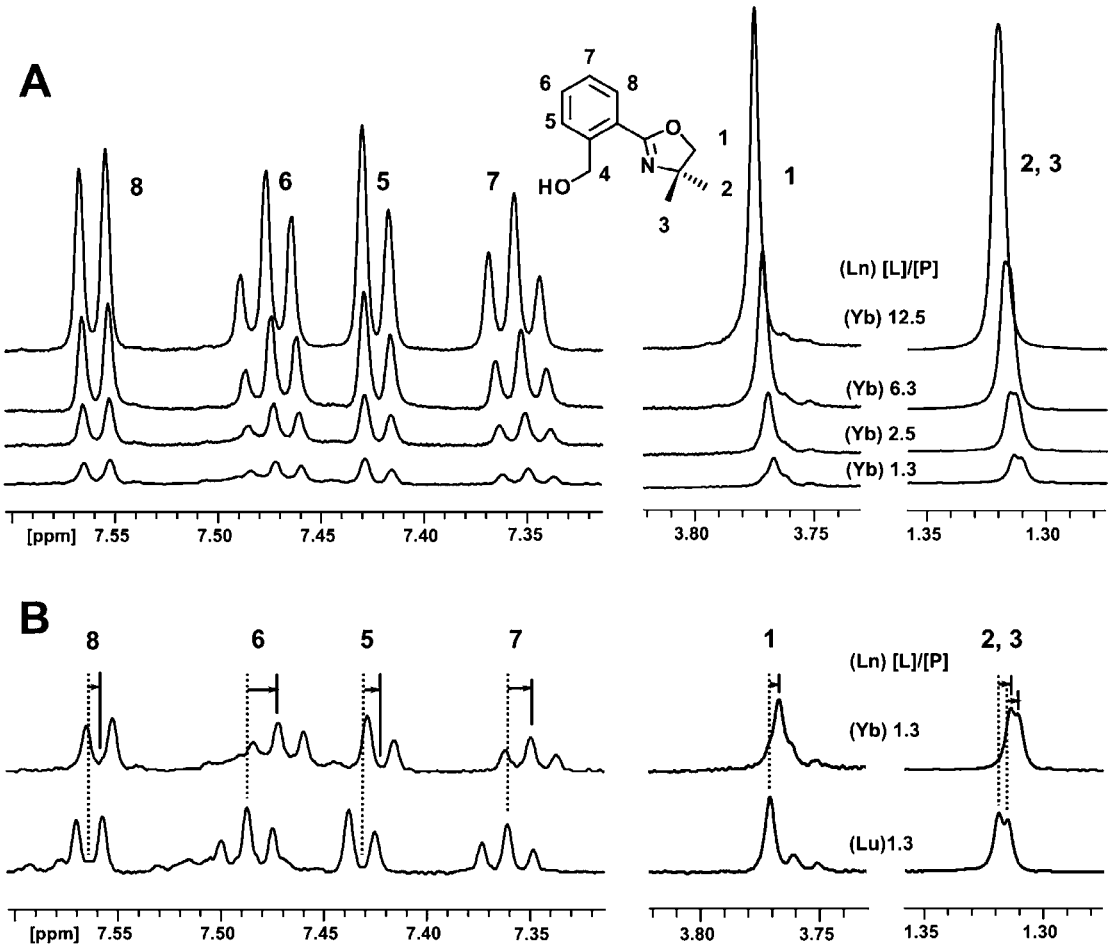

Figure 3. (A) Overlay of 1D ^{1}H NMR spectra of ligand **1** in the presence of 28 μM FKBP12 (34C/35C) attached to paramagnetic Yb^{3+}-CLaNP-5 with increasing ligand/protein molar ratios, which are indicated in the spectra. Proton assignments of **1** are indicated by corresponding numbers on the structure. The chemical shift of proton 4 overlapped with the water resonance and is not shown here. The resonances of the methyl groups numbered 2 and 3 are degenerate in the free form but are resolvable in the bound form. (B) The observed ligand PCS is the difference between the resonance positions for the paramagnetic (Yb^{3+}) and diamagnetic (Lu^{3+}) samples. The dashed and solid lines indicate the positions of the diamagnetic and paramagnetic ligand resonances, respectively. Spectra were recorded at 600 MHz.

conformation is the preferred bound conformation in solution. A possible explanation is that the hydroxyl group from the aromatic ring may form a hydrogen bond with the nitrogen atom, creating an extra 7-membered ring.[42]

Selection of CLaNP-5 Tagging Sites. In order to determine the protein−ligand complex, we also utilized paramagnetic NMR and generated three FKBP12 mutant proteins tagged with the synthetic lanthanide tag CLaNP-5. The lanthanide tag, CLaNP-5, is designed to covalently link to the protein surface via two disulfide bridges.[13,14] Therefore, the presence of surface accessible cysteine pairs is essential. Several criteria need to be considered for selecting the mutation sites: (1) The cysteines should be far enough from the putative ligand binding site to avoid interference with binding, yet close enough to yield appreciable paramagnetic effects: 15−30 Å is a reasonable estimation based on the location of the binding site and the total size of FKBP12; 25 Å is an estimation of the effective range for Yb^{3+}-chelated CLaNP-5. In this study, the distances between the putative ligand binding site and the three lanthanide tags are in the range of 15−25 Å. It is possible to use other lanthanides to adjust the effective range for different protein sizes.[43] (2) The two Cα atoms from the cysteines should be 6−10 Å apart, with their side chains pointing away from the protein surface and roughly in the same direction. Cysteines buried inside the protein cannot react with CLaNP-5. The locations of cysteine mutation sites (K34C/K35C, K44C/K47C, and E61C/Q65C) were selected to satisfy the above requirements. As a consequence of the anisotropy of the magnetic susceptibility, the ligand PCSs can be close to zero regardless of the distance if the ligand is located close to the region in which the PCS changes its sign. Nevertheless, measuring PCSs in this situation for a different tag position will provide information. This is one of the advantages of synthetic tags compared with the methods using lanthanide-binding peptides[44,45] or metal displacement, in which usually only one tag position is available.

Ligand PCS Measurement. The resonance assignments of the free ligand **1** were obtained by analysis of 1D ^{1}H,^{13}C-APT, [^{1}H,^{13}C]-HSQC, and [^{1}H,^{13}C]-HMBC spectra. To eliminate interference from the protein resonances, 1D ^{1}H NMR spectra of the ligand in the presence of Ln^{3+}-CLaNP-5-FKBP12 were recorded using a T_2 relaxation delay of 60 ms. Ligand PCSs were measured from singly tagged protein with Yb^{3+}-CLaNP-5 in the paramagnetic sample and Lu^{3+}-CLaNP-5 in the diamagnetic sample. In total, three different pairs of protein samples, each containing the CLaNP-5 attached at a different

dx.doi.org/10.1021/ja401323m | J. Am. Chem. Soc. 2013, 135, 5859−5868

site, were used. Initially **1** was titrated into Yb^{3+}-CLaNP-5-FKBP12 to determine the optimal molar ratio of protein to ligand. The ligand and protein concentrations were 36 and 28 μM (34C/35C), 24 and 17 μM (44C/47C), and 47 and 39 μM (61C/65C). Under these conditions 0.9−1.9% of the ligand is bound. A protein-to-ligand ratio of 1:1.3 was used for all measurements with both Yb^{3+}-CLaNP-5 and Lu^{3+}-CLaNP-5, because this ratio represented the best compromise between size of the PCSs, the line broadening and spectral resolution. Figure 3 shows the spectra from which the ligand PCSs were determined for the 34C/35C tagging site.

The observed ligand PCS values are small (less than 10 Hz) due to the small fraction of bound ligand (1.5%). However, they can be measured precisely because of the sharp signals of the ligand. The PCSs are summarized in Figure 4. A control

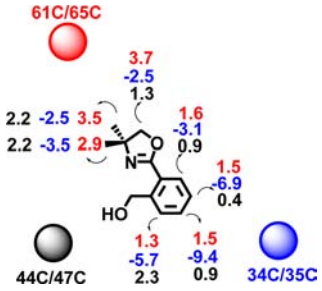

Figure 4. Observed ^{1}H PCS values (in Hz, for spectra acquired at 600 MHz) of ligand **1** from three different locations of the paramagnetic center. The relative positions of the paramagnetic centers are indicated and the associated PCS values are color coded. Blue, PCSs from 34C/35C; black, PCSs from 44C/47C; red, PCSs from 61C/65C.

measurement of the ligand in the presence of the free probe in the absence of protein showed no paramagnetic effects (data not shown). This indicates that the observed ligand PCSs derive exclusively from the bound state of the ligand. A total of 21 PCS values were obtained from the three pairs of para- and diamagnetic spectra.

PCS-Based Structure Calculation with Predicted Δχ-Tensors. For ligands in fast-exchange on the NMR time-scale (i.e., $\Delta\Omega < k_{off}$), the observed PCSs are weighted averages of the free and bound states. Therefore, the PCS values for the bound state can be derived if the fraction of ligand bound is known. Using the known concentration of ligand and protein, as well as the experimentally determined K_D, the observed PCSs were converted to the PCSs in the bound state (Supporting Information, Table S2).

Previous work in which CLaNP-5 was bound to a rigid protein suggested that lanthanide position and the Δχ-tensor orientation can be predicted using a simple set of rules.[14] This characteristic is important for proteins that cannot be isotopically labeled, so we first determined the structure of the complex of **1** bound to FKBP12 using the predicted Δχ-tensor orientations. As with the NOE-based structure determination, several structures of FKBP12 from the PDB were used as input. PDB file 1FKR model 14 is shown as an example. In the docking procedure, the ligand was allowed to move, and the protein was fixed, except for side chains within 8 Å of the ligand, which were allowed to rotate. The complex formed by FKBP12 and ligand **1** was energy minimized guided by the energy terms for the PCSs and Lennard-Jones potential. The five lowest energy structures were selected, based on the total energy and overlaid with the structure derived from NOE restraints (Figure 5). Two orientations are found with low PCS energy, which differ by a rotation of ∼90°; the lower energy

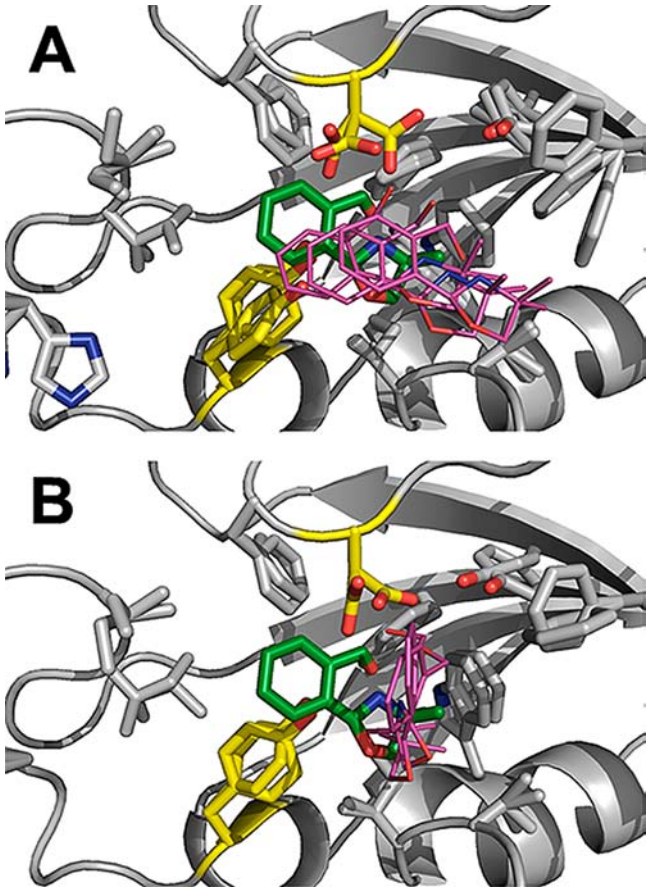

Figure 5. Best five PCS structures calculated using the predicted Δχ-tensors (ligands in magenta) superimposed on the averaged NOE structure (ligands in green). Two clusters with similar PCS energy are present with the ligand rotated by ∼90°. (A) The lowest energy cluster has an orientation parallel to the NOE structure. (B) The second cluster has the aromatic ring pointing out from the binding site.

cluster (Figure 5A) is closest to the orientation observed in the NOE structure. The average RMSD relative to the NOE structure is 4.7 ± 0.9 Å. In the other orientation, which has on average 10% higher PCS energy, the aromatic ring of **1** points outward from the binding site (RMSD relative to NOE 4.4 ± 0.1 Å).

By applying the predicted Δχ-tensor parameters for PCS-based structure calculations, the approximate location of the ligand binding site could be established. Both clusters of calculated orientations showed good agreement between the predicted and experimental ligand PCSs (Figure 6A,B), as indicated by the quality factor (eq 4). This suggests that, using CLaNP-5 with predicted Δχ-tensor parameters, it is possible to detect the ligand binding site and obtain a low-resolution structure for further ligand optimization. For this approach, prediction of the Δχ-tensor position and orientation does not require any PCSs or other NMR data on the protein, although the 3D structure of the protein is required.

Δχ-Tensor Calculations. PCS values depend on the position of the nuclear spin relative to the magnetic susceptibility anisotropy tensor of the lanthanide ion, as described by eq 3 in Materials and Methods. The Δχ-tensors

dx.doi.org/10.1021/ja401323m | J. Am. Chem. Soc. 2013, 135, 5859−5868

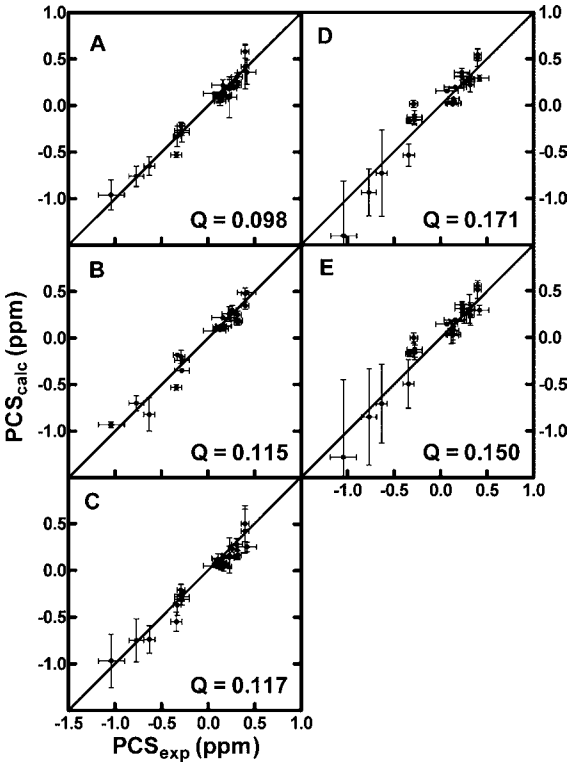

Figure 6. Correlation between experimental and back-calculated ligand PCSs for the top five structures of **1** bound to FKBP12 as determined from predicted and experimentally determined $\Delta\chi$-tensor positions. Correlation of the best structures obtained with predicted $\Delta\chi$-tensors: (A) lowest energy cluster, as shown in Figure 5A, and (B) second lowest energy cluster, as shown in Figure 5B. (C) Best five structures with experimentally determined $\Delta\chi$-tensors. (D) Back-calculated ligand PCS values for NOE-based structures using predicted $\Delta\chi$-tensor positions. (E) Back-calculated ligand PCS values for NOE-based structures using experimentally determined $\Delta\chi$-tensor positions. Vertical error bars represent 2× standard deviation of the variation in the sets of structures for the back-calculated PCSs. Horizontal error bars represent the estimated experimental error.

are defined by eight parameters (the axial and rhombic components, the *x, y, z* coordinates of the metal, and the orientation of the $\Delta\chi$-tensor relative to the molecular frame, defined as three Euler angles). Therefore, they can be determined from a minimum of eight PCSs measured from the nuclear spins with known resonance assignment. The PCS values of protein amide protons were measured as the difference in the chemical shift between the Yb^{3+}- and Lu^{3+}-CLaNP-5 attached FKBP12. Most of the [^{1}H,^{15}N]-HSQC assignments of the wild-type FKBP12 could be transferred to the double cysteine mutants attached to the Lu^{3+}-CLaNP-5. Although there are ambiguous assignments in the spectra of the mutants, more than 70% of the residues could readily be assigned and therefore the $\Delta\chi$-tensor magnitude and orientation could be determined for each of the three mutants. The calculated parameters are summarized in Table 1. Overlays of the paramagnetic and diamagnetic [^{1}H,^{15}N]-HSQC spectra of the three mutants and the correlations between the experimental and back-calculated protein PCSs can be found in Figure S5. Compared with FKBP12 variants K34C/K35C and K44C/K47C, C22V/E61C/Q65C exhibits somewhat smaller tensor magnitudes (Table 1) and a slightly poorer fit (Figure S5), which is an indication that the tag at this position

Table 1. $\Delta\chi$-Tensor Parameters of Yb^{3+}-CLaNP-5 Attached to FKBP12[a]

mutant	K34C/K35C	K44C/K47C	C22V/E61C/Q65C
$\Delta\chi_{ax}$ (10^{-32} m^3)	8.7 ± 0.4	8.9 ± 0.2	7.8 ± 0.1
$\Delta\chi_{rh}$ (10^{-32} m^3)	3.4 ± 0.4	3.3 ± 0.3	2.7 ± 0.2
Q (eq 4)	0.023	0.021	0.035
restraints	75	73	72

[a]Errors were estimated by randomly excluding 10% of the data with a Monte Carlo approach.[29]

is a little more mobile than at the other two positions. Nevertheless, all the values of the axial and rhombic components from three tagging sites are comparable to previously reported values,[14,46−50] and therefore the values for C22V/E61C/Q65C were considered reasonable.

PCS-Based Structure Calculation with Experimentally Determined $\Delta\chi$-Tensors. The docking of ligand **1** to FKBP12 was repeated using the experimentally determined tensor orientations. The orientations of the best five structures form a single cluster that is close to the NOE-derived structure (Figure 7). The correlation of experimental and back-calculated

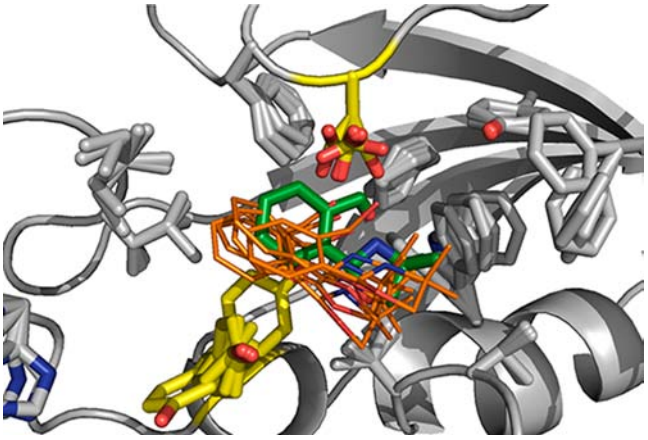

Figure 7. Superposition of the averaged NOE structure (in green) of the FKBP12-**1** complex and the best five structures (in orange) calculated using ligand PCSs and the three experimentally determined $\Delta\chi$-tensors. The protein backbone is represented as a gray ribbon except for the residues D37 and Y82. The average RMSD of the ligand from PCS calculations relative to the NOE calculation is 2.8 ± 0.4 Å.

ligand PCSs is presented in Figure 6C. The average RMSD between the cluster members is 1.6 ± 0.5 Å and to the averaged NOE structure 2.8 ± 0.4 Å. With the experimental $\Delta\chi$-tensor parameters, the quality factor has slightly increased to 0.117. Given the error estimates shown in Figure 6, we conclude that the calculated structures fit the data and that the differences of the Q values between the clusters derived from the predicted and experimental $\Delta\chi$-tensors are not significant. The position of the ligand found with the optimized $\Delta\chi$-tensors is closer to the NOE-based position, suggesting that the optimization increases the accuracy of the solution. The PCSs were also back-calculated from the NOE-based structures, using both the predicted $\Delta\chi$-tensors (Figure 6D) and the experimentally determined $\Delta\chi$-tensors (Figure 6E). It is clear that the NOE-derived ligand position fits the PCS data worse than the calculated position, indicating that the two positions differ significantly from the experimental point of view. The NOE-based structure is used here as the standard for validation of the

dx.doi.org/10.1021/ja401323m | J. Am. Chem. Soc. 2013, 135, 5859−5868

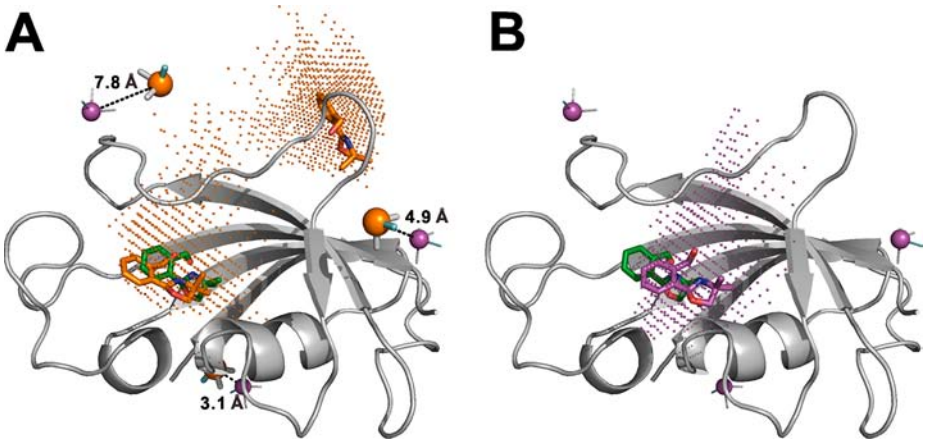

Figure 8. Grid points produced by PCSdock (Q = 0.15). The metal positions are shown in spheres (magenta, predicted positions; orange, experimentally determined positions), and $\Delta\chi$-tensor orientations are shown in sticks, with the z-axis in cyan. Ligands in green are the NOE-based position. (A) The two ligands in orange show the two locations determined by the experimental $\Delta\chi$-tensors. Two clusters were determined by PCSdock (orange dots): one close to the actual binding site, and the other at the "ghost" position. Distances between the metal positions determined by pure prediction and by experimental PCS are indicated. (B) Ligand in magenta shows the position determined using the predicted tensors. Only one cluster was found by PCSdock (magenta dots).

PCS-based structure, but, as mentioned above, the NOE-based solution is also an approximation due to the dynamics in the binding site.

A "Ghost" Site Found by PCS Due to Degeneracy of $\Delta\chi$-Tensors. A commonly encountered problem in paramagnetic NMR is the observation of multiple structure solutions due to the degeneracy of $\Delta\chi$-tensor frames.[51−53] Here, we encountered a similar situation. In the calculations, another cluster of ligands was found at a site entirely different from the one shown in Figure 7 and which was neither identified by any intermolecular NOE, nor reported in the literature. Using the predicted $\Delta\chi$-tensor parameters, this position was not identified. The position is located near a loop consisting of amino acids S39 to F46, opposite to the binding site mentioned above (Figure S6). At this "ghost" site, the ligand has no van der Waals contacts with the protein and is exposed on the protein surface, and therefore it does not appear to be physically realistic. This nonphysical position is apparently an artifact which originates from the degenerate nature of the $\Delta\chi$-tensors. By removing solutions that have zero van der Waals energy, it is possible to eliminate this artifact.

In order to visualize the degeneracy in a set of three tags, a script named PCSdock was written to produce a grid around the protein and calculate the PCS values of the predefined tags for each grid point. The algorithm then compares the experimental PCSs with the three calculated ones and calculates a Q value (eq 5). If the Q value for any atom of the ligand is below a threshold, that grid point is selected; otherwise, it is discarded. Thus, PCSdock gives a fast, though crude, representation of where the ligand could be located on the basis of the PCSs. While the procedure is likely to overestimate the number of possible locations, it can be a useful tool for establishing degeneracy. Applied to FKBP12 with the three tags and the experimentally observed PCSs, the calculation clearly shows two possible, spatially distinct areas (Figure 8A). Each of the two low-energy clusters from the calculation using experimentally determined $\Delta\chi$-tensors fits into one of the areas defined by the PCSdock calculation. Interestingly, this "ghost" site was not found when calculated using the predicted $\Delta\chi$-tensors (Figure 8B).

DISCUSSION

We have demonstrated a general method to obtain structural information on complexes of weakly binding, small-molecule ligands and proteins. The method seems most applicable to proteins that cannot be isotopically labeled, for which X-ray crystallography fails and for which many ligands need characterization. Although powerful, the method has certain limitations. On the target side, proteins with many surface-exposed cysteine residues are not appropriate as it would be quite challenging to attach the CLaNP-5 tag at one unique position. There are also restrictions on the ligands such that those with symmetric structures, with many scalar couplings or that exhibit intermediate exchange on the NMR time scale can cause difficulties in analyzing the data. Ligands that have symmetric structures tend to show degeneracy in NMR spectra, resulting in a reduced number of restraints that are themselves degenerate. Ligands with many scalar couplings, such as a saturated hydrocarbon ring, have ^{1}H spectra that can be difficult to resolve and the PCSs may be difficult or impossible to measure. Similarly, ligands in intermediate-exchange are difficult to study in NMR due to NMR line broadening leading to resonance overlap or less visible resonances. It should be noted that such ligands will present a challenge to any paramagnetic NMR approach, not just those based on the use of a lanthanide tag.

If the goal is to precisely define the binding site of the ligand on the protein, it is essential to obtain a sufficient number of meaningful restraints. Due to their small volume, fragments can only generate restraints covering a limited part of $\Delta\chi$-tensor space, easily leading to degenerate solutions. We addressed this issue by attaching CLaNP-5 at several sites throughout the protein surface. Three tag positions were used to generate a total of 21 PCS restraints for structure calculations. It is also possible to use CLaNP-5 with different lanthanides at a single tagging site, an approach used in previous studies for which multiple $\Delta\chi$-tensor positions were not available.[11,12] However, the tensor orientations of different lanthanides are similar in the same tag, so the PCSs merely scale with the magnitude of the anisotropy, reducing the information content of the extra restraints. In this case, a combined application of CLaNP-5 and

dx.doi.org/10.1021/ja401323m | J. Am. Chem. Soc. 2013, 135, 5859−5868

CLaNP-7[50] would be possible using the same tag position, because the $\Delta\chi$-tensor orientations differ between these two CLaNP molecules. We expected that the three tagging sites would lead to a unique solution for the binding site. Unfortunately, degeneracy remained, leading to a physically unrealistic binding site in addition to the correct site. While the relevant site could be readily distinguished from the irrelevant one, some caution must nevertheless be exercised when interpreting the results. The presence of this "ghost" site suggests that, depending on the actual situation, more than three mutants might be required to fully break all degeneracy. Additionally, it is important to consider the (potential) dynamic behavior of sites within the protein when selecting positions to generate the dual cysteine mutations. Motion of the attachment site within the protein can influence both the position of the paramagnetic center and magnitude of the $\Delta\chi$-tensor.[13,47] For example, the large difference between the predicted and experimental position of the lanthanide for FKBP12 (K34C/K35C) and the orientation of its tensor (Figures 8A and S7) is likely related to its location on an ill-defined protein loop, which makes the prediction less reliable and bears the risk that the tag slightly affects the average structure of the loop.

A number of NMR approaches have been proposed to determine the structure of protein−small molecule complexes. The approach based on intermolecular NOEs, which is robust and provides structural detail, is most frequently used. The method emphasizes short-range restraints (<5 or <8 Å, depending on the isotopic labeling scheme) and requires resonance assignments of the protein. With the assistance of computational modeling, the NOE method can be relatively fast, as demonstrated in the system of matrix metalloproteinases (MMPs) and its tight-binding ligands.[54] A particular limitation of the method is the requirement for isotope-labeled protein, typically necessitating expression in *E. coli*. In contrast, methods that exclusively observe the NMR spectrum of the ligand can, in principle, be applied to protein derived from nearly any source. Epitope mapping, a method that quantitates the amplitude of ligand resonances in a saturation transfer difference spectrum,[55,56] can provide information on how the small molecule binds to the protein. In theory, this information could be used for constraining molecular docking efforts. However, significant artifacts can be introduced by the inherent differences in transverse relaxation rates of ligand resonances. Therefore, the most significant advantage of the paramagnetic methods is that structural information relative to a fixed point on the protein can be reliably obtained from the ligand spectra. Previous paramagnetic NMR methodologies for determining protein−ligand structures have been limited to metalloproteins with an intrinsic metal binding site[12] or have used a lanthanide tag that can only be placed at the N-terminus of a protein.[11] In contrast, the CLaNP-5 tag can be used on non-metalloproteins and can be placed at a variety of sites on the protein, provided they are sufficiently rigid. It should be noted that in our hands, the effect of the tag on the stability of the protein is variable. In some cases, but not certainly not all, the protein more easily precipitates, perhaps due to the partly hydrophobic nature of the cyclen ring system. In general we design several extra double Cys mutants and use the most stable ones. The tag is attached via disulfide bridges, which means that the probe can be lost. The rate of dissociation is variable (days−weeks), so we prepare the samples freshly or store them at −80 °C.

The principle of the proposed technique is based on determination of the ligand position with respect to the paramagnetic $\Delta\chi$-tensors. In order to predict the $\Delta\chi$-tensor positions, the protein structure must be available. The results presented in this study have demonstrated that, with the predicted $\Delta\chi$-tensor parameters, it is possible to identify the ligand binding site. It is not necessary to have protein resonance assignments in order to predict the $\Delta\chi$-tensor position and therefore the approach can be applied to proteins that cannot be readily isotopically labeled. In principle, the approach can also be applied to proteins for which experimental structure information is not available, providing reliable structure prediction methods (such as homology modeling[57,58]) are applicable. For drug discovery, the potential binding site can be identified, which can accelerate optimization of hits to achieve higher affinity and greater biological activity even when the structure of the target is not available.

■ CONCLUSIONS

We have successfully determined the site and orientation of a small-molecule ligand binding to a protein using ligand PCS and validated the results with an NOE structure. The use of the CLaNP-5 tag to induce the paramagnetic effects makes this approach suitable for non-metalloproteins. The results show that this strategy can identify the ligand binding site better than chemical shift perturbations. Comparison of the PCS structures from predicted and experimentally determined tensors demonstrates that the predicted tensor positions are sufficient for coarse definition of the binding site, and it is therefore not necessary to experimentally optimize the tensor position. This PCS-based approach can be useful in early stages of fragment-based drug discovery to identify binding sites for proteins that are difficult to enrich with isotopes, and in this way support optimization of early fragment hits.

■ ASSOCIATED CONTENT

Supporting Information

NOESY spectra showing intermolecular NOEs; list of NOE restraints used for NOE-based structure calculations; NOE-based structures from various PDB structures; correlation between the experimental PCSs and the back-calculated PCSs for all three $\Delta\chi$-tensor positions; [^{1}H,^{15}N]-HSQC overlay of paramagnetic and diamagnetic spectra; list of ligand PCSs used in the PCS-based structure calculation; figure showing the "ghost" site; Sanson−Flamsteed projections of the predicted and experimental tensors; and the PCSdock script. This material is available free of charge via the Internet at http://pubs.acs.org.

■ AUTHOR INFORMATION

Corresponding Author

m.ubbink@chem.leidenuniv.nl; g.siegal@chem.leidenuniv.nl

Notes

The authors declare the following competing financial interest(s): G.S. acknowledges >5% ownership of ZoBio, a company that provides research services in drug discovery.

■ ACKNOWLEDGMENTS

Financial support from the Netherlands Organisation for Scientific Research, grants 700.58.405 (P.H.J.K.), and 700.58.441 (W.-M.L., S.P.S., and M.U.). Financial support by the Access to Research Infrastructures activity in the 7th

Framework Programme of the EC (Project number: 261863, Bio-NMR) for conducting the research is gratefully acknowledged. H.S. is a member of the DFG-funded cluster of excellence: macromolecular complexes.

REFERENCES

(1) Hajduk, P. J.; Greer, J. *Nat. Rev. Drug Discovery* **2007**, *6*, 211−219.
(2) Schieborr, U.; Vogtherr, M.; Elshorst, B.; Betz, M.; Grimme, S.; Pescatore, B.; Langer, T.; Saxena, K.; Schwalbe, H. *ChemBioChem* **2005**, *6*, 1891−1898.
(3) Keizers, P. H. J.; Ubbink, M. *Prog. Nucl. Magn. Reson. Spectrosc.* **2011**, *58*, 88−96.
(4) Otting, G. *Annu. Rev. Biophys.* **2010**, *39*, 387−405.
(5) Otting, G. *J. Biomol. NMR* **2008**, *42*, 1−9.
(6) Bertini, I.; Fragai, M.; Lee, Y.-M.; Luchinat, C.; Terni, B. *Angew. Chem., Int. Ed.* **2004**, *43*, 2254−2256.
(7) Jahnke, W.; Rüdisser, S.; Zurini, M. *J. Am. Chem. Soc.* **2001**, *123*, 3149−3150.
(8) Jahnke, W.; Perez, L. B.; Paris, C. G.; Strauss, A.; Fendrich, G.; Nalin, C. M. *J. Am. Chem. Soc.* **2000**, *122*, 7394−7395.
(9) Zhuang, T.; Lee, H.-S.; Imperiali, B.; Prestegard, J. H. *Protein Sci.* **2008**, *17*, 1220−1231.
(10) Gochin, M.; Zhou, G.; Phillips, A. H. *ACS Chem. Biol.* **2011**, *6*, 267−274.
(11) Saio, T.; Ogura, K.; Shimizu, K.; Yokochi, M.; Burke, T. R.; Inagaki, F. *J. Biomol. NMR* **2011**, *51*, 395−408.
(12) John, M.; Pintacuda, G.; Park, A. Y.; Dixon, N. E.; Otting, G. *J. Am. Chem. Soc.* **2006**, *128*, 12910−12916.
(13) Keizers, P. H. J.; Desreux, J. F.; Overhand, M.; Ubbink, M. *J. Am. Chem. Soc.* **2007**, *129*, 2−5.
(14) Keizers, P. H. J.; Saragliadis, A.; Hiruma, Y.; Overhand, M.; Ubbink, M. *J. Am. Chem. Soc.* **2008**, *130*, 14802−14812.
(15) Michnick, S. W.; Rosen, M. K.; Wandless, T. J.; Karplus, M.; Schreiber, S. L. *Science* **1991**, *252*, 836−839.
(16) Van Duyne, G. D.; Standaert, R. F.; Karplus, P. A.; Schreiber, S. L.; Clardy, J. *Science* **1991**, *179*, 839−842.
(17) Wandless, T. J.; Michnick, S. W.; Rosen, M. K.; Karplus, M.; Schreiber, S. L. *J. Am. Chem. Soc.* **1991**, *113*, 2339−2341.
(18) Brath, U.; Akke, M. *J. Mol. Biol.* **2009**, *387*, 233−244.
(19) Van Duyne, G. D.; Standaert, R. F.; Karplus, P. A.; Schreiber, S. L.; Clardy, J. *J. Mol. Biol.* **1993**, *229*, 105−124.
(20) Petros, A. M.; Kawai, M.; Luly, J. R.; Fesik, S. W. *FEBS Lett.* **1992**, *308*, 309−314.
(21) Vanwetswinkel, S.; Heetbrij, R. J.; van Duynhoven, J.; Hollander, J. G.; Filippov, D. V; Hajduk, P. J.; Siegal, G. *Chem. Biol.* **2005**, *12*, 207−216.
(22) Kneller, T. D.; Goddard, D. G. *SPARKY 3*.
(23) Worrall, J. A. R.; Reinle, W.; Bernhardt, R.; Ubbink, M. *Biochemistry* **2003**, *450*, 7068−7076.
(24) Kannt, A.; Young, S.; Bendall, D. S. *Biochim. Biophys. Acta* **1996**, *1277*, 115−126.
(25) Güntert, P.; Mumenthaler, C.; Wüthrich, K. *J. Mol. Biol.* **1997**, *273*, 283−298.
(26) Burkhard, P.; Taylor, P.; Walkinshaw, M. D. *J. Mol. Biol.* **2000**, *295*, 953−962.
(27) Szep, S.; Park, S.; Boder, E. T.; Van Duyne, G. D.; Saven, J. G. *Proteins* **2009**, *74*, 603−611.
(28) Bertini, I.; Luchinat, C.; Parigi, G. *Prog. Nucl. Magn. Reson. Spectrosc.* **2002**, *40*, 249−273.
(29) Schmitz, C.; Stanton-Cook, M. J.; Su, X.-C.; Otting, G.; Huber, T. *J. Biomol. NMR* **2008**, *41*, 179−189.
(30) Schwieters, C. D.; Kuszewski, J. J.; Tjandra, N.; Marius Clore, G. *J. Magn. Reson.* **2003**, *160*, 65−73.
(31) Banci, L.; Bertini, I.; Cavallaro, G.; Giachetti, A.; Luchinat, C.; Parigi, G. *J. Biomol. NMR* **2004**, *28*, 249−261.
(32) Schüttelkopf, A. W.; Van Aalten, D. M. F. *Acta Crystallogr.* **2004**, *D60*, 1355−1363.
(33) Bashir, Q.; Volkov, A. N.; Ullmann, G. M.; Ubbink, M. *J. Am. Chem. Soc.* **2010**, *132*, 241−247.
(34) Jones, E.; Oliphant, T.; Peterson, P. *SciPy: Open Source Scientific Tools for Python*; 2001
(35) Shuker, S. B.; Hajduk, P. J.; Meadows, R. P.; Fesik, S. W. *Science* **1996**, *274*, 1531−1534.
(36) Sapienza, P. J.; Mauldin, R. V; Lee, A. L. *J. Mol. Biol.* **2011**, *405*, 378−394.
(37) Schrödinger, L. *The PyMOL Molecular Graphics System*, Version 0.99.
(38) Cheng, J.-W.; Lepre, C. A.; Moore, J. M. *Biochemistry* **1994**, *33*, 4093−4100.
(39) Cheng, J.-W.; Lepre, C. A.; Chambers, S. P.; Fulghum, R.; Thomson, J. A.; Moore, J. M. *Biochemistry* **1993**, *32*, 9000−9010.
(40) Brath, U.; Akke, M.; Yang, D.; Kay, L. E.; Mulder, F. A. A. *J. Am. Chem. Soc.* **2006**, *128*, 5718−5727.
(41) Liang, J.; Choi, J.; Clardy, J. *Acta Crystallogr., Sect. D: Biol. Crystallogr.* **1999**, *55*, 736−744.
(42) Chuang, W.-T.; Hsieh, C.-C.; Lai, C.-H.; Lai, C.-H.; Shih, C.-W.; Chen, K.-Y.; Hung, W.-Y.; Hsu, Y.-H.; Chou, P.-T. *J. Org. Chem.* **2011**, *76*, 8189−8202.
(43) Keizers, P. H. J.; Ubbink, M. In *Protein NMR Spectroscopy: Practical Techniques and Applications*; Lian, L.-Y., Roberts, G., Eds.; John Wiley & Sons, Ltd.: Chichester, UK, 2011; pp 193−219.
(44) Wöhnert, J.; Franz, K. J.; Nitz, M.; Imperiali, B.; Schwalbe, H. *J. Am. Chem. Soc.* **2003**, *125*, 13338−13339.
(45) Martin, L. J.; Hähnke, M. J.; Nitz, M.; Wöhnert, J.; Silvaggi, N. R.; Allen, K. N.; Schwalbe, H.; Imperiali, B. *J. Am. Chem. Soc.* **2007**, *129*, 7106−7113.
(46) Xu, X.; Keizers, P. H. J.; Reinle, W.; Hannemann, F.; Bernhardt, R.; Ubbink, M. *J. Biomol. NMR* **2009**, *43*, 247−254.
(47) Hass, M. A. S.; Keizers, P. H. J.; Blok, A.; Hiruma, Y.; Ubbink, M. *J. Am. Chem. Soc.* **2010**, *132*, 9952−9953.
(48) Bertini, I.; Calderone, V.; Cerofolini, L.; Fragai, M.; Geraldes, C. F. G. C.; Hermann, P.; Luchinat, C.; Parigi, G.; Teixeira, J. M. C. *FEBS Lett.* **2012**, *586*, 557−567.
(49) Dasgupta, S.; Hu, X.; Keizers, P. H. J.; Liu, W.-M.; Luchinat, C.; Nagulapalli, M.; Overhand, M.; Parigi, G.; Sgheri, L.; Ubbink, M. *J. Biomol. NMR* **2011**, *51*, 253−263.
(50) Liu, W.-M.; Keizers, P. H. J.; Hass, M. A. S.; Blok, A.; Timmer, M.; Sarris, A. J. C.; Overhand, M.; Ubbink, M. *J. Am. Chem. Soc.* **2012**, *134*, 17306−17313.
(51) Longinetti, M.; Parigi, G.; Sgheri, L. *J. Phys. A: Math. Gen.* **2002**, *35*, 8153−8169.
(52) Bertini, I.; Longinetti, M.; Luchinat, C.; Parigi, G.; Sgheri, L. *J. Biomol. NMR* **2002**, *22*, 123−136.
(53) Saio, T.; Yokochi, M.; Kumeta, H.; Inagaki, F. *J. Biomol. NMR* **2010**, *46*, 271−280.
(54) Bertini, I.; Fragai, M.; Giachetti, A.; Luchinat, C.; Maletta, M.; Parigi, G.; Yeo, K. J. *J. Med. Chem.* **2005**, *48*, 7544−7559.
(55) Mayer, M.; Meyer, B. *Angew. Chem., Int. Ed.* **1999**, *35*, 1784−1788.
(56) Mayer, M.; Meyer, B. *J. Am. Chem. Soc.* **2001**, *123*, 6108−6117.
(57) Pavlopoulou, A.; Michalopoulos, I. *Int. J. Mol. Med.* **2011**, *28*, 295−310.
(58) Dhaliwal, B.; Chen, Y. W. *Infect. Disord. Drug Targets* **2009**, *9*, 557−562.